THERMOGRAVIMETRIC ANALYSIS OF THERMAL INSULATING MATERIALS EXPOSED TO SODIUM VAPOR

Raymond Luneng[1], Zhaohui Wang[1,2], Arne Petter Ratvik[2], Tor Grande[1]

1. Department of Materials Science and Engineering, NTNU Norwegian University of Science and Technology, NO-7491 Trondheim, Norway.
2. SINTEF Industry, NO-7465 Trondheim, Norway.
Corresponding author: raymond.luneng@ntnu.no

Keywords: Thermal Insulating Materials; Aluminum Electrolysis Cell; Sodium Vapor; Thermogravimetric Analysis

Abstract

The bottom thermal insulating layer in aluminum electrolysis cells is normally well protected from chemical attacks by a refractory layer. However, autopsies of spent cathode lining have shown that sodium vapor may reach and react with the thermal insulating layer, thus affecting the thermal balance and structural integrity of the entire electrolysis cell. Here, we report on a new laboratory test, named Na-tg test, where commercial thermal insulating materials are exposed to sodium vapor at controlled temperature and sodium partial pressure. The weight change of three commercial insulation materials was measured as a function of time at various temperatures and partial pressures of sodium. The exposed materials were investigated with respect to changes in the microstructure, chemical and mineralogical composition, due to the reaction with sodium. The findings are discussed with respect to the chemical durability of the three thermal insulating materials.

Introduction

The bottom thermal insulating layer is important for the thermal balance and structural stability of aluminum electrolysis cells. This layer is typically made of diatomaceous earth (Moler), calcium silicate, or vermiculite based materials, which have a very high porosity and thus a low thermal conductivity [1,2]. The low thermal conductivity strongly reduces heat loss through the bottom of the cell, but the low density makes them vulnerable to damage from molten aluminum, bath components, or any volatile species they may come in contact with [3]. The much denser aluminosilicate-based refractory layer, on top of the insulation, is designed to protect against chemical attacks from corrosive bath components. However, degradation of the bottom cell lining is normally initiated by sodium [4,5]. Formation of sodium vapor occurs naturally in the electrolysis process, and is therefore unavoidable, by the following reactions at the cathode [4]:

$$Al\ (l) + 3\ NaF\ (\text{in cryolite}) = 3\ Na\ (\text{in C}) + AlF_3\ (\text{in cryolite}) \quad (1)$$

or

$$Na^+\ (\text{in electrolyte}) + e^- = Na\ (\text{in C}) \quad (2)$$

The sodium vapor pressure at the cathode depends on the bath chemistry and temperature, but is estimated to be about 0.02-0.03 atm at a temperature of 960 °C [6]. From analysis of spent pot lining, Tschöpe et al. identified a first reaction front in the refractory layer in spent pot linings [5]. This first reaction front was characterized by a high sodium content, while fluorine components originating from the molten electrolyte were found 1-2 cm above the first reaction front. The autopsies demonstrated that sodium vapor is the first volatile species to diffuse through the carbon cathodes and react with the refractory layer. The sodium content in the first reaction front was found to be as high as 16-18 wt% within the first 3-4 mm. Moreover, Tschöpe et al. found that the sodium reaction front had penetrated through roughly 75-100 % of the refractory layer in the cells, demonstrating the ability of sodium vapor to reach the thermal insulation layer.

The stability of the thermal insulating materials have not received much attention in the literature [1,7]. The effects of sodium vapor exposure clearly warrants attention, as the interaction can alter material properties and ultimately the thermal and structural stability of the entire cell. In this work, commercial thermal insulating materials were exposed to sodium vapor in a special thermogravimetric laboratory test [8]. In addition, to record sodium uptake in the materials at controlled conditions, we report on the impact of Na vapor on the chemical and mineralogical durability as well as structural stability of the thermal insulation materials.

Experimental

The materials used in the study were commercially available materials from Skamol A/S. The selected products represent typical materials used for the thermal insulating layer of aluminum electrolysis cells. The calcium silicate material was the SUPER-1100 E, hereby referred to as simply CaSi. The vermiculite material was V1100 (475), hereby referred to as vermiculite. The Moler material was SUPRA, hereby referred to as Moler. Cylindrical samples were machined with a core drilling machine, giving the samples dimensions of 2.4 cm diameter and 7.9 cm height. A 1 mm diameter hole was drilled horizontally through the sample, approximately 0.5 cm from the top of the sample. This allowed a Ni-Cr alloy wire (BRIGHTRAY alloy C, Special Metals) to connect the sample to the electronic balance (WXSS204, Mettler Toledo), recording the weight of the sample.

From the production of the insulation materials, Moler was the only fired product, and therefore loss on ignition (LOI) could have a significant impact on the weight change of the materials during testing. To avoid this and limit the weight change to reaction with sodium vapor during testing, the samples were heated to 850 °C and held for 12 h in a separate oven, and subsequently stored in a desiccator prior to the thermogravimetric analysis.

The experimental setup for the Na thermogravimetric test, referred to as Na-tg test, has previously been reported by Wang et al. for investigation of sodium vapor interaction with carbon cathode materials [8]. A schematic drawing of the Na-tg experimental setup is illustrated in Figure 1. After connecting the sample to the balance, metallic sodium (Sigma Aldrich, CAS number 7440-23-5) was placed at the bottom of the reactor tube. The reactor tube was evacuated three times by a rotary pump to 10^{-2} mbar, with argon gas flushing through the reactor tube in between each evacuation. The reactor tube was filled with approximately 240 mbar argon gas before starting the experiment, as this would prevent the sodium from boiling in heating zone 2. The sample was heated to the experimental temperature, T_{sample}, of 800 °C before heating of the sodium was initiated, in order to remove any contribution to the weight change due to the thermal treatment. Two different experiments were performed for each material. While T_{sample} was held constant at 800 °C for both experiments, the temperature in heating zone 2 around the sodium source, T_{Na}, was varied in the range 500-700 °C, thus affecting the partial pressure of Na. In the first experiment, referred to as exp. 1, the sodium in heating zone 2 was held at T_{Na} = 500 °C, and the exposure lasted 24 h. In the second experiment, referred to as exp. 2, T_{Na} was first 600 °C for 18 h, and directly increased to T_{Na} = 700 °C for another 18 h. The experimental conditions for exp. 1 and exp. 2 are listed in Table 1 for reference, including calculated sodium partial pressures from Equation (3) [9]:

$$\ln p = 11.9463 - 12633.73/T - 0.4672 \ln T \qquad (3)$$

where T is temperature in K and p is sodium vapor pressure given in MPa.

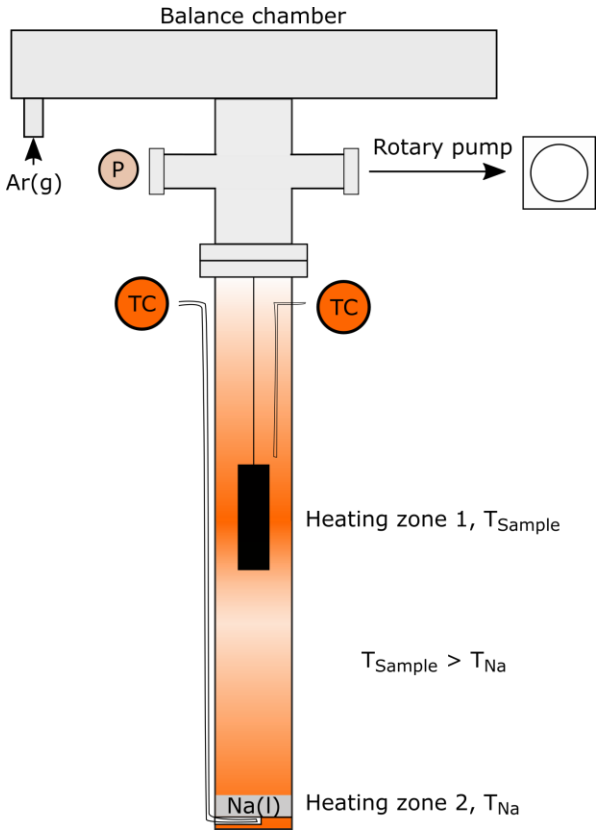

Figure 1. Schematic of the experimental thermogravimetric analysis setup (not to scale).

Table 1. Experimental conditions for the two experiments, referred to as exp. 1 and exp. 2. For both experiments T_{sample} = 800 °C.

	T_{Na} [°C]	Na partial pressure [atm]	Time [h]
Exp. 1	500	0.005	24
Exp. 2	600/700	0.0335/0.141	18/18

A digital caliper was used to measure the diameter (measured on top, middle, and bottom of the sample) and height of the samples both before and after the Na-tg test. The cylindrical samples were investigated after the Na-tg test by visual inspection, X-ray diffraction (Bruker AXS D8 Focus), and scanning electron microscopy (SEM) and energy-dispersive X-ray spectroscopy (EDS), using the Zeiss Ultra 55 Limited

Edition. Horizontal slices of the cylindrical samples were embedded in epoxy and subsequently polished for SEM and EDS investigation. Electron back-scattering mode was used on the SEM to enhance the elemental contrast of the samples. The polished cross sections of the samples were made approximately 1.5 cm above the bottom of the sample, in order to eliminate the edge effect from the bottom. Thus, the Na penetration depth into the sample was limited to the radial direction.

Results

The thermogravimetric analysis of the samples during exposure to Na vapor are shown in Figure 2.

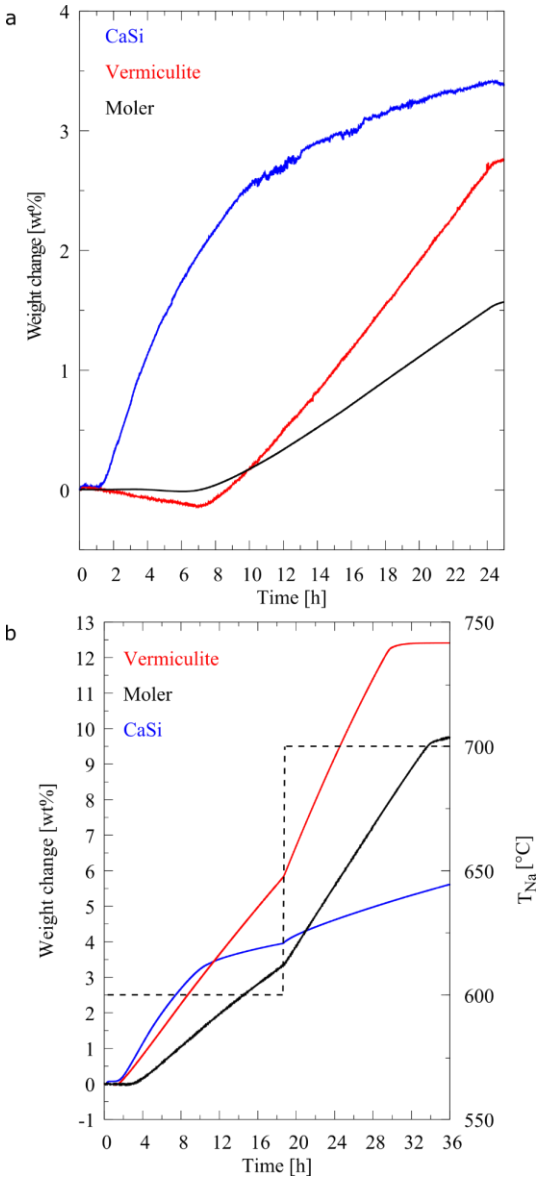

Figure 2. Weight change of the three materials as function of time during exposure to Na. a) exp. 1, b) exp. 2, where T_{Na} given by dotted line showing T_{Na} changed from 600 °C to 700 °C at ~18 h. In both a) and b), the materials are listed from highest to lowest total weight change at the end of the test.

Figure 2 a) shows the thermogravimetric analysis from exp. 1, where T_{Na} was held constant at 500 °C for 24 h. The Moler and vermiculite samples demonstrate an almost linear weight increase, while a parabolic-shaped curve is observed for CaSi. The initial slope is also higher for CaSi. The thermogravimetric analysis for exp. 2 is shown in Figure 2b), where T_{Na} was first held at 600 °C for 18 h and then instantly increased to 700 °C for another 18 h. T_{Na} is illustrated by the dotted line. The same parabolic shape is observed for the weight gain that was observed for CaSi during the first 18 h, while a more linear weight increase is observed for the last 18 h. The almost linear weight increase for both Moler and vermiculite is observed throughout exp. 2. However, the slope increases significantly at ~18 h, when T_{Na} was increased from 600 °C to 700 °C. The flattening of the curve at the end of exp. 2 for both Moler and vermiculite is likely due to depletion of the sodium source, as the samples reacted with more sodium than anticipated.

The loss on ignition (LOI) from pre-heating the samples before the experiments, as well as the weight increase after the Na-tg test are listed in Table 2. LOI is significant for both vermiculite and CaSi, as the materials were not fired to high temperatures during fabrication.

Table 2. Weight change [wt%] of all samples after the initial heat treatment (LOI) and after the Na-tg test.

	LOI [wt%]	**Na-tg weight change [wt%]**
Moler exp. 1	-0.56	1.57
Moler exp. 2	-0.57	9.75
Vermiculite exp. 1	-4.02	2.75
Vermiculite exp. 2	-3.96	12.41
CaSi exp. 1	-11.98	3.38
CaSi exp. 2	-11.91	5.62

The dimensional changes of the cylindrical samples measured after the test are summarized in Table 3. The samples were measured prior to the Na-tg test (named pre-exp. 1/2), and after the Na-tg test.

Table 3. Diameter ⌀ and height of the samples measured before (pre-exp.) and after each experiment.

	Upper ⌀ [mm]	**Middle ⌀ [mm]**	**Lower ⌀ [mm]**	**Height [mm]**
Moler				
Pre-exp. 1	23.50	23.87	23.42	79.01
Exp. 1	23.49	23.87	23.40	78.61
Pre-exp. 2	23.88	23.97	23.91	78.99
Exp. 2	23.82	21.74	21.56	77.96
Vermiculite				
Pre-exp. 1	23.20	23.17	23.27	78.98
Exp. 1	23.18	23.21	23.31	78.79
Pre-exp. 2	23.08	23.24	23.12	78.97
Exp. 2	22.77	22.22	22.68	77.60
CaSi				
Pre-exp. 1	23.98	24.09	23.95	78.39
Exp. 1	23.58	24.05	23.34	78.38
Pre-exp. 2	24.07	24.08	23.94	78.35
Exp. 2	24.09	24.12	23.41	78.25

The visual appearance of the Moler samples after the Na-tg test is shown in Figure 3, where the pristine material (a) is displayed for comparison. Fracture cross sections from roughly 1.5 cm above the bottom of the samples from exp. 1 and exp. 2 are also provided in Figures 3 b)-c). The black, glassy, outer reaction layer (Rx-layer) is clearly seen, being more prominent for exp. 2 than for exp. 1. A glassy, round "ball" (not shown here) was found at the lower edge of the cylinder in the exp. 2 sample, below the point where the polished cross section was made.

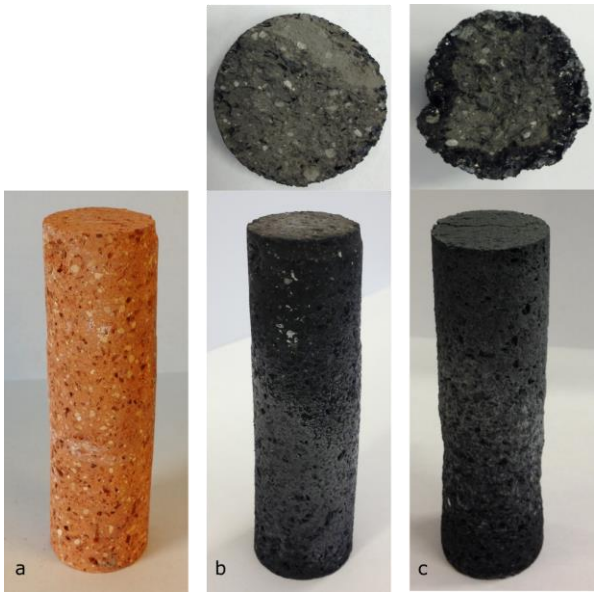

Figure 3. Macroscopic observations of pristine Moler (pre-exp. 1) in a), exp. 1 sample with a fracture cross section in b), and exp. 2 sample with a fracture cross section in c). Note the visible, glassy outer Rx-layer in the cross sections.

SEM micrographs of the Moler samples from exp. 1 and exp. 2 are shown in Figure 4 a)-b) and 4 c)-d), respectively. A distinct reaction layer is evident in both samples, Figure 4 a) and c). The black color in the images comes from the epoxy the samples are embedded in, thus corresponding to pores/voids in the microstructure. The sodium distribution is shown in red in Figure 4 b) and d), measured by EDS elemental mapping. Clear gradients and variations in the Na content were observed going from the outside towards the center, in line with expectations.

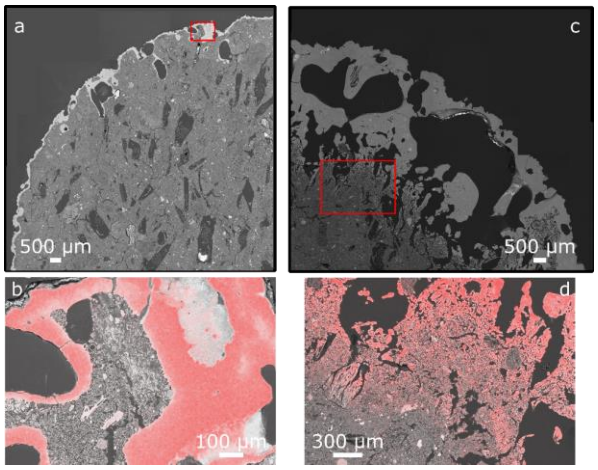

Figure 4. SEM micrographs of the polished cross sections of the Moler samples a)-b) exp. 1, and c)-d) exp. 2. Red area in b) and d) from EDS Na mapping.

Figure 5 shows the visual appearance of the vermiculite samples after the Na-tg test in b) and c), in addition to the pristine material in a). The cross section of the sample from exp. 1 (b) shows a clear outer Rx-layer, with an inner core resembling the pristine material. An outer Rx-layer can also be seen for the sample from exp. 2 (c), but with a black inner core.

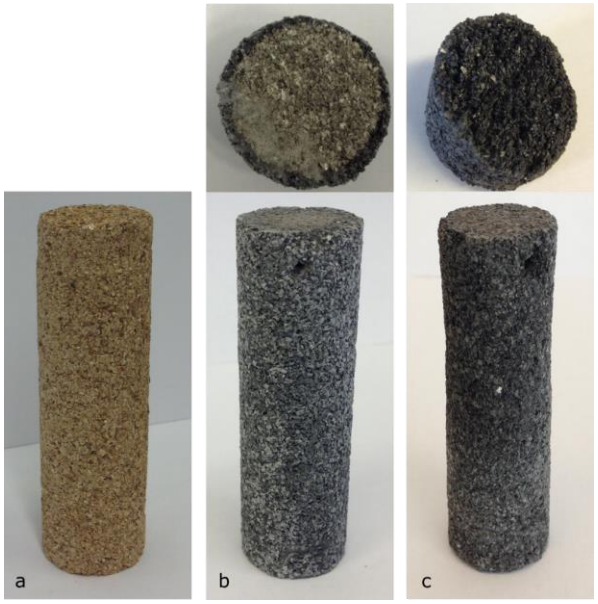

Figure 5. Macroscopic observations of pristine vermiculite in a), exp. 1 sample with a fracture cross section in b), and exp. 2 sample with a fracture cross section in c). In b), note the visible outer Rx-layer in the cross section as well as the inner core with similar appearance as the pristine material.

SEM micrographs of the vermiculite samples are shown in Figure 6 a)-b) and 6 c)-d) for exp. 1 and exp. 2, respectively. The characteristic parallel sheet structure of the vermiculite grains is mostly observed in the sample from exp. 1 while several denser grains are observed in the inner core of the sample from exp. 2. The inner core of the exp. 2 sample is observed to have large voids, as opposed to the inner core of exp. 1 sample. The Na distribution in the outer Rx-layer of the exp. 1 sample, as measured by EDS, is shown with red color in Figure 6 b). This shows that the sodium is mostly concentrated in the outer Rx-layer corresponding to the visible layer in the cross section of Figure 5 b). Na mapping of the sample from exp. 2 is shown in Figure 6 d) and shows sodium present in both the outer Rx-layer and inner core.

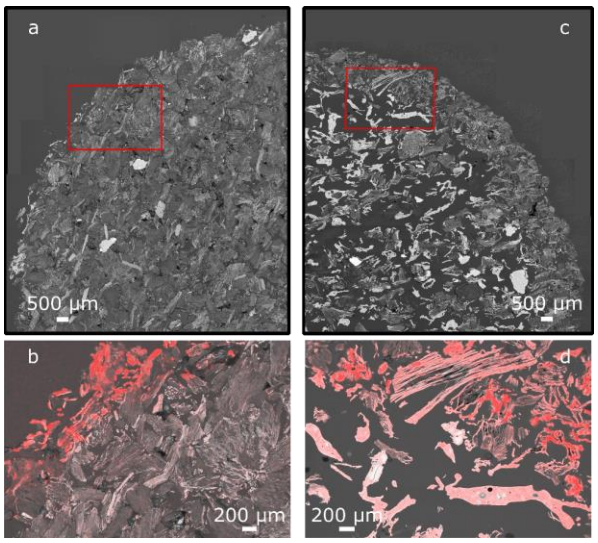

Figure 6. SEM micrographs of the polished cross sections of the vermiculite samples for exp. 1 in a) and b), and exp. 2 in c) and d). Note the coarser grain structure of the inner core of the exp. 2 sample.

Figure 7 shows the visual appearance of the CaSi samples, with the pristine material displayed for comparison in a). Exp. 1 and exp. 2 are shown in b) and c), respectively. For both cross sections in b) and c), a thin outer Rx-layer is visible. This Rx-layer was observed to be very brittle and would easily fall off during handling of the sample. The cracks in this layer, observed at the bottom of the exposed samples, were observed right after the experiments were completed and not caused by handling of the samples.

SEM micrographs of the sodium exposed CaSi samples are shown in Figure 8 a)-b) and 8 c)-d) for exp. 1 and exp. 2, respectively. For exp. 1, the brittle outer Rx-layer can barely be observed in the overview of Figure 8 a), while it is seen more clearly with EDS Na mapping shown by red color in b). For exp. 2, the outer Rx-layer is only partially covering the overview of the sample in Figure 8 c), as the brittle nature of this layer made it difficult to preserve around the entire sample. In Figure 8 c), a small outer part of the Rx-layer can be seen to appear a little brighter than the rest of the Rx-layer. A closer look at the microstructure of the material at this borderline is shown in Figure 9 by imaging of a fracture surface of the sample. The thin, characteristic needle structure of CaSi is observed below this borderline, while the microstructure is visibly coarser above it.

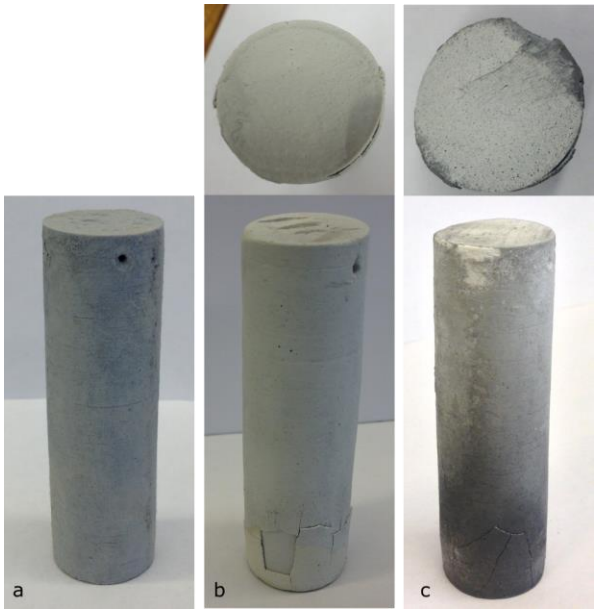

Figure 7. Macroscopic observations of pristine CaSi in a), exp. 1 sample with a fracture cross section in b), and exp. 2 sample with a fracture cross section in c). Note the thin, fractured outer Rx-layer in the cross sections.

The major phases of the different materials as identified by XRD are summarized in Table 4. Both pristine material and thermal reference samples are listed, in addition to the exposed samples. Measurements were made for both the visible outer Rx-layer as well as the inner core

of the sodium exposed samples. CaSi and vermiculite are not thermally stable with respect to the mineralogy, as new phases are formed after heat-treatment. In both Moler and vermiculite samples exposed to sodium vapor, iron oxide is reduced to either metallic iron or various iron-silicon phases. In addition, the presence of an amorphous and/or nano-crystalline phase was evident for the Moler sample as observed previously [10]. The phases observed in the glassy "ball" found at the bottom of the exp. 2 sample of Moler are also listed in the table, marked with a star (*).

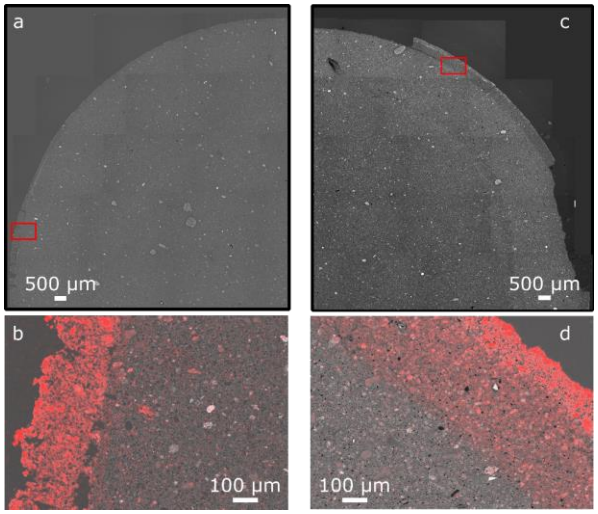

Figure 8. SEM micrographs of polished cross sections of the CaSi samples. Exp. 1 shown in a) and b), and exp. 2 shown in c) and d). Red area in b) and d) from EDS Na mapping.

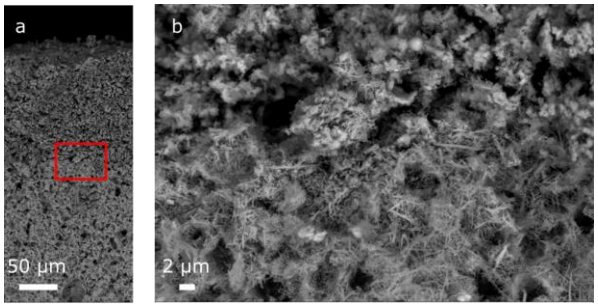

Figure 9. SEM micrographs of CaSi exp. 2 fracture surface.

Discussion

The importance of pre-heating the materials before the test is evident by comparing the numbers for LOI and Na-tg test weight gain in Table 2. If the samples were not pre-heated, the true weight gain from Na interaction would not be attained, and comparison of the different materials would be impossible as the Na uptake would not be possible to distinguish from LOI. The sodium partial pressure in the experiments was controlled indirectly by adjusting T_{Na}, and the Na pressure was calculated by using Equation (3). Thus, the sodium partial pressure was approximately 0.005 atm during exp. 1, and 0.0335-0.141 atm during exp. 2. From the estimated sodium partial pressures at the cathode of 0.02-0.03 atm in real electrolysis cells [6], the conditions of exp. 2 are close to the maximum Na activity, while the conditions in exp. 1 represent a situation further down in the lining as the sodium partial pressure will inevitably decrease down the lining. Exp. 2 can serve as an accelerated sodium exposure test, showing the impacts of prolonged sodium exposure. The comparison of the two tests also give valuable information with respect to the reaction mechanisms of the materials with sodium vapor at two different temperatures.

Table 4. Major phases identified by XRD in pristine material, thermal reference samples, and samples from exp. 1 and exp. 2. For pristine and therm. ref. samples there is no outer Rx-layer or inner core.

	Outer Rx-layer	**Inner core**
Moler – pristine	-	SiO_2 (quartz) Fe_2O_3
Moler – therm. ref.	-	SiO_2 (quartz) Fe_2O_3
Moler – exp. 1	SiO_2 (quartz) Fe	SiO_2 (quartz) Fe
Moler – exp. 2	SiO_2 (quartz) Fe	SiO_2 (quartz) Fe

	Fe_3Si	FeSi* $FeSi_2$*
Vermiculite – pristine	-	Phlogopite
Vermiculite – therm. ref.	-	Phlogopite Mg_2SiO_4 $KAlSi_2O_6$
Vermiculite – exp. 1	Mg_2SiO_4 $NaAlSiO_4$ $KAlSiO_4$ Fe	Phlogopite Mg_2SiO_4 Fe
Vermiculite – exp. 2	$NaAlSiO_4$ Fe_3Si Fe	Mg_2SiO_4 $NaAlSiO_4$ $KAlSiO_4$ Fe_3Si
CaSi – pristine	-	$Ca_6Si_6O_{17}(OH)_2$
CaSi – therm. ref.	-	$CaSiO_3$
CaSi – exp. 1	$Na_2Ca_2Si_2O_7$ Na_2CaSiO_4	$CaSiO_3$
CaSi – exp. 2	$Na_2Ca_2Si_2O_7$	$CaSiO_3$

*: Phases identified by XRD of the glassy, round "ball" found at the bottom of the Moler exp. 2 sample.

The test method allows independent adjustment of T_{Sample} and sodium partial pressure by T_{Na} (as long as $T_{Sample} > T_{Na}$, to avoid condensation of sodium). This opens up the possibility for investigating the materials under various conditions, e.g. at lower T_{Sample} as one moves further down the lining. The real-time recording of sample weight, T_{Sample}, and T_{Na} also give the benefit of quantifiable data about the ongoing interaction of sodium vapor with insulating materials, as opposed to a previous laboratory test by the authors where the Na vapor pressure could not be controlled and kept constant during the test [10]. The thermogravimetric analysis thus contributes to the understanding of sodium vapor interaction with the materials.

The graphs in Figure 2 show an almost linear weight increase for both the Moler and vermiculite samples at all T_{Na}. The flattening of the curve at the end of exp. 2 for both Moler and vermiculite is likely due to depletion of the sodium source, as the samples reacted with more sodium than anticipated. However, a parabolic shape is observed for the CaSi samples at T_{Na} = 500-600 °C, while it increases linearly as T_{Na} was increased to 700 °C in exp. 2. The weight increase of the CaSi samples initiates at the same time in both experiments, while it takes a longer time for the Moler and vermiculite samples in exp. 1 compared to exp. 2. This is likely an experimental artifact possibly related to an oxide scale on the surface of the sodium metal, as the sodium partial pressure at the specific temperature should be reached quite rapidly in the reactor tube. The small initial weight decrease for vermiculite in exp. 1 is not expected and is most likely due to some experimental artifact.

The dimensional changes of the samples listed in Table 3 show that the Moler and vermiculite samples after exp. 2 are more severely affected compared to the samples after exp. 1. The shrinkage in diameter in exp. 2 for both Moler and vermiculite is also visually seen in Figures 3 c) and 5 c), and indicates, when coupled with the severe coarsening of the microstructure seen in Figures 4 c) and 6 c), formation of a liquid phase during the experiments. The glass ball found at the bottom of the exp. 2 Moler sample is clear evidence of the presence of a liquid phase, which becomes glassy during cooling.

The dimensional changes of the CaSi samples show similar results for both experiments. Most of the shrinkage in the CaSi samples is seen in the lower diameter, where the brittle reaction layer is most prominent. The mineralogy in the inner core of the CaSi samples (Table 4) does not change from the thermal reference, and EDS mapping shows that Na is largely contained in the outer Rx-layer (Figure 8), which points to the shrinkage being linked to the change in mineralogy in the outer Rx-layer and coarsening of microstructure (Figure 9). The parabolic shape of the graph in the thermogravimetric analysis (Figure 2) could point to Na saturation, formation of a barrier layer, or a decrease in reaction kinetics.

The phases identified by XRD (Table 4) show no Na-containing phases for the exposed Moler samples, and the only mineralogical change is the reduction of iron oxide to metallic iron or various iron-silicon phases. This demonstrates that sodium is concentrated in the viscous, glassy phase formed during the experiments. Thermodynamic equilibrium calculations of the Moler material with increasing amounts of sodium vapor predicts the following sequence for reduction of the iron oxide: Fe, Fe_3Si, FeSi, $FeSi_2$ [11]. This sequence corresponds well with the mineralogy observed in the various parts of the samples from exp. 1 and exp. 2 (including the glass ball). The finding of metallic iron, instead of iron oxide, in the inner core of both exp. 1 and exp. 2, show that sodium has penetrated the entire samples. The sodium content in the inner core is sufficiently high to reduce the iron oxide, but not high enough to form the viscous, glassy phase.

The same observation regarding reduction of iron, and the sequence of iron-silicon phases with increasing sodium, is made for the vermiculite samples. Metallic iron is found in the inner core of exp. 1, showing that, as for the Moler material, sufficient amounts of sodium have penetrated the entire sample, even though it visually appears unaffected (Figure 5 b)). Phlogopite, $KAlSi_2O_6$ (leucite) and Mg_2SiO_4 (forsterite) are the phases present before sodium exposure. Leucite is spent before forsterite, as forsterite is still found in most parts of the exposed

samples. This is in agreement with predictions by thermodynamic calculations [11]. The other phases are also mostly consistent with previous findings [10].

The CaSi material shows a complete mineralogical transformation when exposed to the pre heat-treatment, from $Ca_6Si_6O_{17}(OH)_2$ (xonotlite) to $CaSiO_3$ (wollastonite). $Na_2Ca_2Si_2O_7$ and Na_2CaSiO_4 are found in the outer Rx-layer of the exposed samples. $Na_2Ca_2Si_2O_7$ has previously been identified [10], but is not predicted by thermodynamic considerations (Na_2CaSiO_4, as well as $Na_2Ca_2Si_3O_9$ are predicted) [11]. This shows that reaction kinetics play an important role for the interaction of sodium vapor with the CaSi material.

Based on the thermogravimetric analysis and characterization of the exposed materials, CaSi was the material least negatively affected by the sodium vapor at the given conditions. The dimensional changes are limited in both experiments, and sodium is largely distributed to a thin, outer Rx-layer (~300-500 µm). This stands in contrast to previous findings where severe deformation of CaSi by creep was observed at a higher temperature of 970 °C [10], showing that temperature is a crucial factor for the interaction between sodium and thermal insulation materials.

Conclusion

A new thermogravimetric analysis test for investigation of the interaction of sodium vapor with thermal insulating materials was demonstrated. The effect on the microstructure varies for the materials, from formation of a viscous, glassy layer for Moler, to a coarsening of the needle-structure of calcium silicate. The mineralogy of the exposed samples coincides largely with previous findings and thermodynamic equilibrium calculations of sodium vapor interaction [10,11]. However, the Na-tg test provides the benefits of real-time measurements of sample weight, sample temperature, as well as indirect sodium partial pressure. The tunability of the system is invaluable for further investigations of sodium vapor interaction with thermal insulating materials used in the aluminum industry.

Acknowledgement

Financial support from the Norwegian Research Council and Hydro Aluminium, Alcoa Norway, Elkem Carbon and Skamol A/S, through the project CaRMa - Reactivity of Carbon and Refractory Materials used in Metal Production Technology, is gratefully acknowledged.

References

[1] A. L. Yurkov and L. M. Aksel (2005) PROPERTIES OF HEAT-INSULATING MATERIALS (A REVIEW). Refract. Ind. Ceram. 46(3):170–174.
[2] A. Seltveit (1992) Ildfaste materialer. Tapir.
[3] H. Kvande and P. A. Drabløs (2014) The Aluminum Smelting Process and Innovative Alternative Technologies. J. Occup. Environ. Med. 56(5):23–32
[4] M. Sørlie and H. A. Øye (2010) Cathodes in Aluminium Electrolysis, 3rd ed. Aluminium-Verlag Marketing & Kommunikation GmbH, Düsseldorf
[5] K. Tschöpe, C. Schøning, J. Rutlin, and T. Grande (2012) Chemical Degradation of Cathode Linings in Hall-Héroult Cells - An Autopsy Study of Three Spent Pot Linings. Met. Trans. B 43(2):290–301
[6] A. Solheim and C. Schøning (2008) Sodium Vapour Degradation of Refractories Used in Aluminium Cells. Light Metals 967–972
[7] F. B. Andersen and J. Mikkelsen (2000) Thermal Conductivity Measurements of Cathode Insulation Materials. Light Metals 429-435
[8] Z. Wang, A. P. Ratvik, E. Skybakmoen, and T. Grande (2014) Interaction of Sodium Vapor and Graphite Studied by Thermogravimetric Analysis. Light Met. 1239–1244
[9] P. Browning and P. E. Potter (1985) An assessment of the experimentally determined vapour pressures of the liquid alkali metals. In Ohse, R. W. (ed): Handbook of Thermodynamic and Transport Properties of Alkali Metals; Blackwell Scientific Publications, Oxford
[10] R. Luneng, S. N. Bertel, J. Mikkelsen, A. P. Ratvik, and T. Grande (2017) Chemical Stability of Thermal Insulating Materials in Sodium Vapour Environment. Light Metals 543–549
[11] R. Luneng, T. Grande, and A. P. Ratvik (2016) Assessment of the Thermodynamic Stability of Thermal Insulating Materials in Aluminium Electrolysis Cells. Proc. 34th Int. ICSOBA Conf. 1-10